GA–A25252

TURBULENCE BEHAVIOR IN THE PRESENCE OF TRANSPORT BARRIERS

by
K.H. BURRELL

OCTOBER 2005

GENERAL ATOMICS

DISCLAIMER

GA–A25252

TURBULENCE BEHAVIOR IN THE PRESENCE OF TRANSPORT BARRIERS

by
K.H. BURRELL

This is a preprint of a paper to be presented at the 10th IAEA Technical Meeting on H-Mode Physics and Transport Barriers, September 28-30, 2005, in St. Petersburg, Russia, and to be published in the *Plasma Phys. & Control. Fusion.*

Work supported by
the U.S. Department of Energy
under DE-FC02-01ER54698

GENERAL ATOMICS PROJECT 30200
OCTOBER 2005

ABSTRACT

There is general agreement that the creation of transport barriers in magnetized plasmas is associated with the reduction in turbulence-driven transport. The fundamental physics involved in barrier formation are the effects of equilibrium $E \times B$ shear and zonal flows on turbulence and transport. This paper focuses on three major issues in turbulence and transport barriers: 1) Zonal flows and their effects on turbulence, 2) spatial spreading of turbulence from regions of instability to regions of stability, and 3) the effects of short wavelength turbulence. This work gives a short summary of experimental work bearing on each of the themes and, more importantly, raises fundamental questions to motivate future research in each of these areas.

I. INTRODUCTION

Investigation of the physics of the formation of edge and core transport barriers over the past two decades has produced significant insight into the behavior of turbulent transport in magnetized plasmas. This work lead to the development of the model of turbulence suppression by sheared $E \times B$ flow (see review by Terry [1]), which is particularly effective for the essentially two-dimensional turbulence seen in magnetized plasmas. More recently, analogous effects due to oscillating $E \times B$ flows called zonal flows have emerged as an important part of the overall turbulence physics in those plasmas (see review by Diamond et al. [2]).

The present paper focuses on several fundamental themes in turbulence and transport barrier formation, primarily from an experimental viewpoint. These are: 1) zonal flows, 2) spatial spreading of turbulence (nonlocality) and 3) short wavelength turbulence. Each of these is at the frontier of turbulence research in magnetized plasmas. The goal of this work is to give a short summary of experimental work bearing on each of the themes and, more importantly, to raise fundamental questions to motivate future research in each of these areas.

II. ZONAL FLOWS

A. Introduction to zonal flows

Since a recent review [2] has extensively discussed the theory of zonal flows, only a short summary of their characteristics is needed here to make contact with the experimental results. Zonal flows are stable modes driven by the plasma turbulence that then regulate the turbulence amplitude and turbulent transport by shearing apart the turbulent eddies. Accordingly, they are an important part of the overall turbulence picture, since they can have a substantial impact on turbulent transport.

In toroidal geometry, zonal flows come in two types. The first is the low frequency zonal flow which is associated with a toroidally and poloidally symmetric electrostatic potential oscillation with spatial variation in the radial direction only. If one thinks of the structure of this potential in a magnetic flux surface, the poloidal mode number m and the toroidal mode number n are both zero. For the low frequency zonal flow, the relative density fluctuation $\tilde{n}/n$ is much smaller than the relative potential fluctuation $\tilde{\Phi}/eT$. The radial wavenumber k_r of the low frequency zonal flow lies in the range $a\,\rho_i > k_r^{-2} > \rho_i^2$, where a is the plasma minor radius and ρ_i is the ion gyroradius in the toroidal field. Numerical simulations indicate that k_r is about $0.1/\rho_i$, which is somewhat smaller than $1\ \mathrm{cm}^{-1}$ in typical fusion plasmas.

The second type of zonal flow is the Geodesic Acoustic Mode (GAM), which is driven by the low frequency zonal flow owing to the poloidal variation in $E \times B/B^2$. The potential structure of the GAM is also primarily $m/n = 0/0$; however, there is also a significant pressure fluctuation associated with the GAM which has an $m/n = 1/0$ variation within the flux surface. (This $m/n = 1/0$ pressure variation also drives small $m = 1/n = 0$ and higher harmonic sidebands in the potential structure.) Since the low frequency zonal flow and the GAM are coupled, they have radial structures of similar size. Unlike the low frequency zonal flow, the GAM has a specific frequency, given by $f_{GAM} = G\sqrt{(T_e + T_i)/m_i}\,/2\pi R$ [2], where T_e and T_i are the electron and ion temperatures, respectively, m_i is the ion mass, R is the plasma major radius and G is a geometrical factor of order unity.

The GAMs are subject to Landau damping, so their damping rate is given roughly by $\nu = \omega_{GAM} \exp\left(-G^2 q^2/2\right)$ [2]. Here $\omega_{GAM} = 2\pi f_{GAM}$ and q is the magnetic safety

factor. GAMs are relatively more important near the plasma edge where the damping rate is smaller owing to higher local q values.

Because of the nonlinear coupling of the various modes, the low frequency zonal flow, the GAM and the plasma microturbulence amplitudes are all coupled together in a self-consistent feedback loop.

The summary of experimental results presented here confronts two key questions:

1. Is the experimental evidence conclusive enough that we can say that zonal flows have been observed?
2. What are the roles of the low frequency zonal flows and the GAMs in regulating shorter wavelength turbulence? Can the GAM itself regulate turbulence and transport?

B. Experimental results

Some of the clearest data on zonal flows comes from the Compact Helical System (CHS) stellarator. This device has a unique capability to measure density and electrostatic potential fluctuations with long toroidal correlation lengths by using a pair of heavy ion beam probes separated toroidally by 90 degrees [3-5]. Each beam probe makes measurements at three nearby radial locations. As is shown in figure 1, especially at frequencies below 1 kHz, there is significant toroidal coherence in the electrostatic potential fluctuations; these exhibit a phase shift of zero between the two measurement locations. This is consistent with the $n = 0$ structure expected for zonal flows. In addition, by considering the relative locations of the probe points on the flux surface, the experiments have tested the $m = 0$ prediction over a 30 deg to 50 deg range in poloidal angle. Furthermore, as is shown in figure 1(c), there is a coherent oscillation at a frequency of about 16.5 kHz, which is quite close to the theoretically expected frequency for the GAM.

The radial structure of the low frequency zonal flow potential measured in CHS is shown in figure 2. This is obtained by two different cross coherence techniques [3] using data where the radius of one measurement point is moved relative to the other. The potential varies radially with a scale of 1-2 cm. This is in the range theoretically expected for the zonal flow.

The results in figure 3 show how the zonal flow can modulate the higher frequency density and potential fluctuations [5]. This demonstrates a portion of the self-consistent feedback loop of low frequency zonal flows, GAMs and microturbulence. Figure 3(a) shows the time history of the potential difference between two neighboring radial points, giving a visual indication of how the electric field E_r varies in time. When this difference is positive, the E_r from the zonal flow enhances the equilibrium E_r,

increasing the overall $E \times B$ shear. As can be seen in figures 3(b) and 3(c), this leads to a reduction in the density fluctuations between 100 and 170 kHz and to a reduction in the electrostatic potential fluctuations in the 30 to 70 and 100 to 170 kHz ranges. The reason for the different frequency ranges for the effect on the density and potential fluctuations is as yet unexplained.

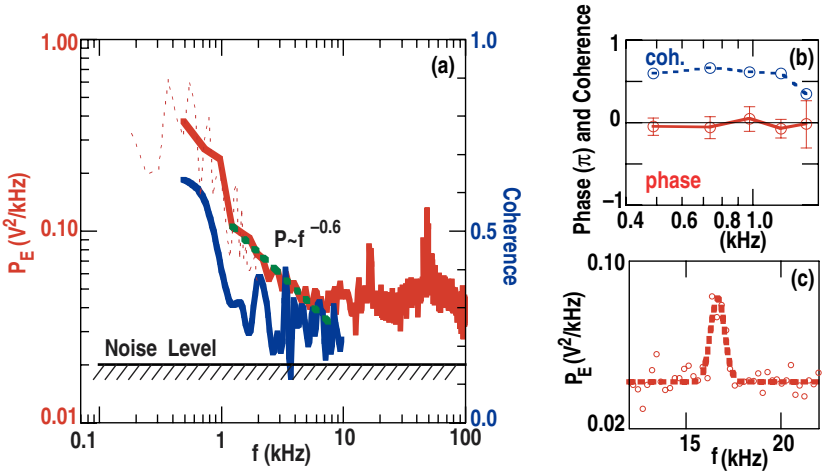

Fig. 1. Data from CHS showing (a) power spectra of potential difference (red lines), and coherence between potential differences (blue line) at the two toroidal locations. The electric field fluctuation ranging from 0.3 to 1 kHz shows long-range correlation, and reflects the activity of the zonal flow of nearly zero frequency. The hatched region shows the noise level for power. (b) An example of phase (divided by π) and coherence between potential differences at two toroidal locations on a magnetic flux surface. (c) An expanded view of a sharp peak at f = 16.5 kHz.

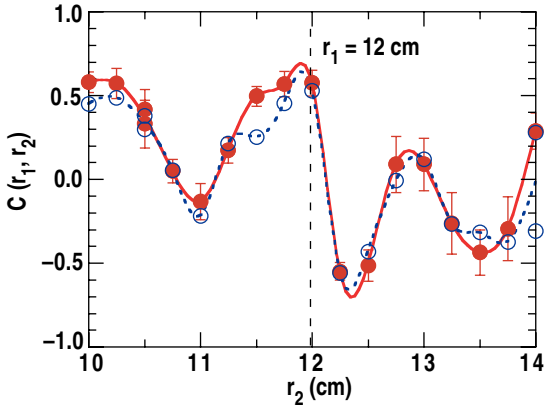

Fig. 2. Radial structure of zonal flow in CHS. The structure is estimated from correlation between potential differences at different toroidal locations. In this experiment, the observation radius of the second HIBP is varied around r_2 = 12 cm with the observation point of the first HIBP being fixed at r_1 = 12 cm. The closed circles represent the traditional correlation coefficient as a function of the observation radius of the second HIBP, while the open circles show the coherent structure.

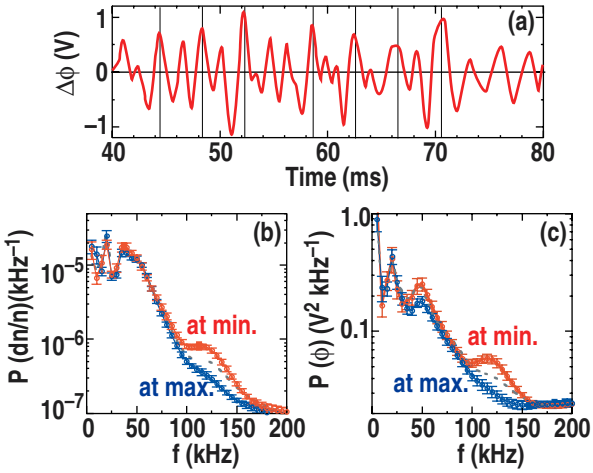

Fig. 3. Causal relationship between turbulence and zonal flow. (a) Temporal evolution of zonal flow. (b) Density and (c) potential fluctuation spectra in the time windows discriminated by zonal flow amplitude; i.e., maxima, zero and minima.

Data showing another part of the self-consistent feedback loop of low frequency zonal flows, GAMs and microturbulence comes from edge measurements with Langmuir probes in JFT2-M [6]. As is illustrated in figure 4, the amplitude of the coherent edge oscillation in the GAM frequency range is modulated by the low frequency zonal flows. When the zonal flow amplitude is large, so is the coherent mode amplitude and vice versa. This is what is expected theoretically if low frequency zonal flows drive GAMs.

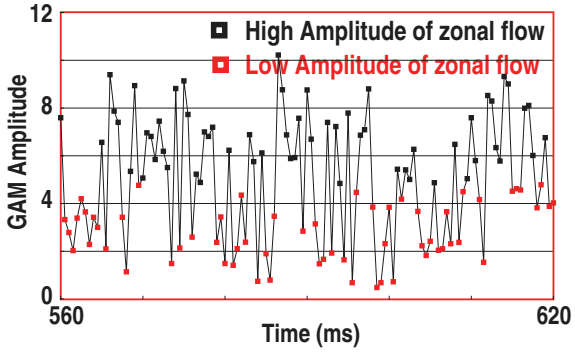

Fig. 4. Langmuir probe data from JFT2-M showing that the amplitude of GAM is modulated by the zonal flow. The plot shows the amplitude of the GAM as a function of time. The points are color coded by the zonal flow amplitude. Black indicates a high amplitude of the zonal flow while red indicates a low amplitude. The correlation is consistent with the theoretical picture that the GAM is driven by the zonal flow.

In tokamaks, the history of GAM observations in a sense actually predates the development of the theory of zonal flows. Early observations on TEXT [7] and JIPP-TIIU [8,9] using heavy ion beam probes saw coherent fluctuations in the GAM

frequency range; however, with no zonal flow theory available, these fluctuations at the time were either unexplained or misidentified [7]. With hindsight, it became clear that the oscillations fit the overall picture of GAMs [10,11]. Later observations in T-10 revealed a similar picture [11]. The frequency of the oscillation scales with temperature as predicted by theory for both TEXT and T-10 [11]. The mode was consistent with an $m = 0$ poloidal mode structure, as determined by multiple poloidal measurements. The radial scale of the mode was similar to or smaller than the 2 cm sample size of the measurements in TEXT and the GAM was seen in the outer portion of the plasma $0.65 \leqq r/a \leqq 0.95$. The spatial scale is consistent with the theoretically predicted spatial scale and the presence of the GAM primarily in the outer portion of the discharge is consistent with the q dependence of the GAM damping rate.

In addition to looking at GAMs using measurements of the electrostatic potential, several groups have investigated them by utilizing the poloidal velocity of the turbulence itself. On ASDEX-Upgrade, this velocity has been measured using Doppler reflectometry which employs launching and receiving horns with a component of line of sight perpendicular to the magnetic field [12]. Frequency analyzing these velocity measurements reveals a coherent velocity oscillation at a frequency near that expected for the GAM. As is shown in figure 5, for a given plasma shape and current, the frequency of this oscillation scales with temperature consistent with the theoretical prediction for GAMs. The frequency changes significantly for the different cases with different vertical elongation κ and q, suggesting that the geometrical factor G can depend strongly on these variables. In the ASDEX-Upgrade data presented in Ref. [12], the coherent oscillation is seen predominantly in the steep density gradient region in the plasma edge. This location may contribute to the strong dependence on κ and q.

On DIII-D, turbulence velocities have also been extracted from two-dimensional measurements of density fluctuations obtained with the beam emission spectroscopy (BES) system using various cross correlation techniques to track the motion of the turbulent eddies [13]. As is shown in figure 6(a), frequency analyzing the poloidal velocity data reveals the presence of a coherent oscillation with frequency about 15 kHz [14-16]. As is seen in figure 6(b), there is little if any poloidal phase variation of this oscillation, demonstrating a poloidal mode number that is definitely $|m| < 2$ and is consistent with $m = 0$. In addition, the radial phase shift shows a 180 deg phase change in a distance of about 2.5 cm. Both the poloidal and radial variation are consistent with the theoretical expectation for the GAM. In addition, the scaling of the frequency of this oscillation with temperature is consistent with the theoretical prediction for the GAM [15,16].

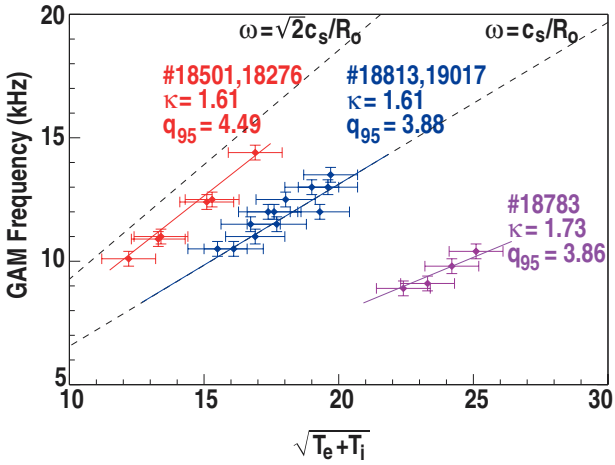

Fig. 5. GAM frequency versus $\sqrt{(T_e + T_i)}$ for selected shots in ASDEX-Upgrade with low elongation κ and high q_{95} (red), medium q_{95} (blue) and high κ (purple). Plasma is a lower single-null divertor discharge operating in the L-mode.

More recent DIII-D BES measurements with an improved detector system have determined the radial profile of the GAM amplitude [17]; this is shown in figure 7. As with the ASDEX-Upgrade result, this is peaked near the plasma edge but extends somewhat further into the plasma. The region where the GAM is seen is the higher q portion of the discharge, where the theoretically predicated GAM damping rate would suggest that the GAM amplitude would be larger. A more direct test of the q dependence of this damping rate is shown in figure 8, where the GAM amplitude is plotted as a function of q_{95} using data taken in a series of current ramp discharges. The amplitude variation is qualitatively consistent with the exponential dependence in the theoretical damping rate.

Very recent DIII-D BES measurements with the improved detector system have now also identified the low frequency zonal flow in the poloidal turbulence velocity spectrum [18]. This low frequency flow has a poloidal variation consistent with $m = 0$ and is seen into $\rho = 0.6$; contrast this to the GAM radial profile seen in figure 8 which shows the GAM amplitude becoming small at $\rho = 0.8$.

The two dimensional nature of the BES data lends itself to studies of the nonlinear energy transfer due to the GAM by utilizing bicoherence analysis [19]. Starting with the continuity equation, one can demonstrate that this nonlinear transfer can be investigated by calculating

$$T_n^y(f, f') = -\mathrm{Re}\left\langle \tilde{n}^*(f)\, V_y(f - f')\, \frac{\partial \tilde{n}}{\partial y}(f') \right\rangle \quad .$$

Here, the y derivative is in the poloidal direction and the V_y is the turbulence velocity in the poloidal direction.

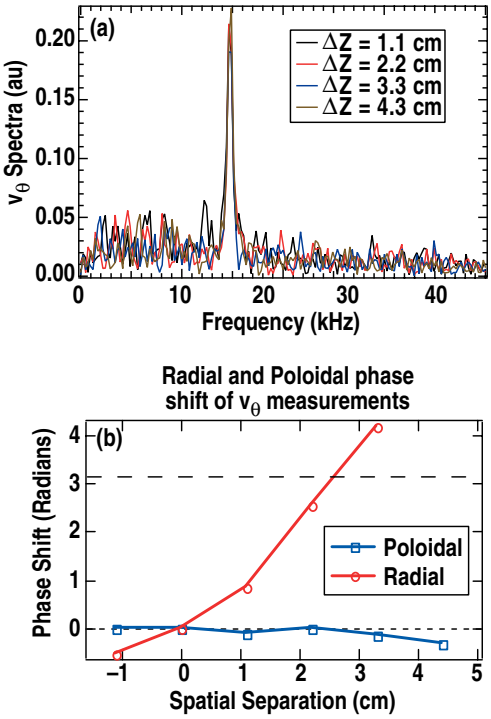

Fig. 6. BES data from DIII-D showing (a) cross-power spectrum of poloidally separated measurements of v_θ(t) indicating coherent poloidal flow oscillation with high spatial and spectral coherence and long poloidal wavelength. (b) Phase relation as a function of radial and poloidal separation for the BES array. Reference measurement is taken in the corner of the array. Velocity oscillation exhibits little or no measurable poloidal phase shift but significant radial phase shift, which gives rise to a flow shear.

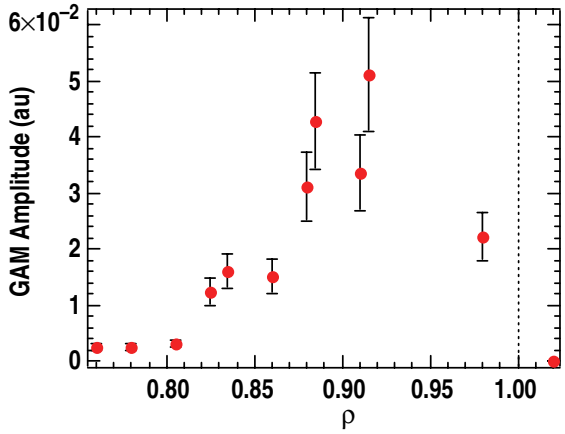

Fig. 7. Radial profile of GAM amplitude determined from BES measurements in DIII-D, indicating strong peaking near $r/a \sim$ 0.9-0.95 with rapid falloff inside and towards separatrix. Measurements obtained during two repeat discharges from t = 1100-1300 ms at I_p = 1.2 MA, q_{95} = 4.7.

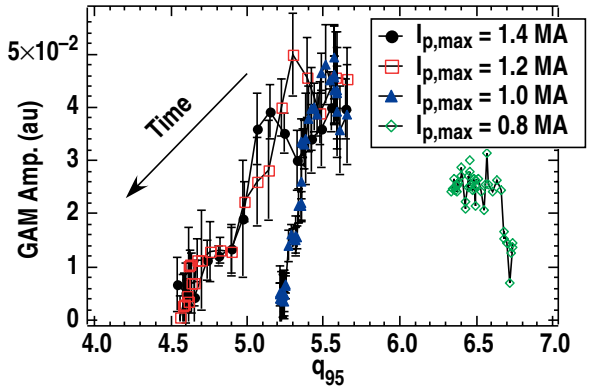

Fig. 8. Relative GAM amplitude measured near $\rho = 0.9$ plotted as a function of q_{95} for four discharges with different maximum plasma current, with each trace compiled from temporal variation within one discharge (at 50 ms intervals). These BES results from DIII-D show the GAM amplitude decreases strongly as q_{95} decreases.

$T_n^y(f, f')$ measures the transfer of energy between density fluctuations at frequency f and poloidal density gradient fluctuations at f' at a specific location. A positive value indicates that $\tilde{n}(f)$ is gaining energy from $\partial\tilde{n}/\partial y(f')$ and a negative value indicates that $\tilde{n}(f)$ is losing energy to $\partial\tilde{n}/\partial y(f')$.

The two-dimensional BES measurements give all the quantities needed to experimentally calculate the portion of $T_n^y(f, f')$ associated with GAM advection. For two points 1 and 2 separated poloidally, we have $\tilde{n}(r, t) = (n_1 + n_2)/2$, $\partial\tilde{n}/\partial y = (n_1 - n_2)/\Delta y$. The GAM velocity can be determined as was done for the previous analysis. Because of the correlation analysis used to extract the GAM velocity, we are able to find experimentally the portion of V_y due to the GAM but not the shorter scale, higher frequency portions related to the microturbulence.

As is shown in figure 9, $T_n^y(f, f')$ clearly shows that fluctuations at $f = f' + f_{GAM}$ gain energy while those that $f = f' - f_{GAM}$ lose energy. In other words, turbulent energy moves between $\tilde{n}$ and $\partial\tilde{n}/\partial y$ in steps of f_{GAM} and there is a net transfer of energy to high frequency. This quantifies that the shearing action of the GAMs leads to a cascade to high frequency.

C. Conclusions on zonal flows and GAMs

The experimental measurements on low frequency zonal flows show

1. An $n = 0$ toroidal structure in CHS.
2. An $m = 0$ poloidal structure in DIII-D and CHS.
3. Modulation of higher frequency turbulence by zonal flows in CHS.
4. Centimeter scale radial structure in CHS.

The experimental measurements on GAMs show

1. An $m = 0$ poloidal structure in DIII-D and TEXT.
2. GAM modulation of higher frequency turbulence in DIII-D.
3. Zonal flow modulation of GAMs in JFT2-M.
4. Centimeter-scale radial structure in DIII-D and TEXT.
5. Temperature dependence of GAM frequency consistent with the theoretical prediction in ASDEX-U, DIII-D, TEXT and T-10.
6. Amplitude variation qualitatively consistent with the q-dependence of the theoretically predicted damping rate in DIII-D.

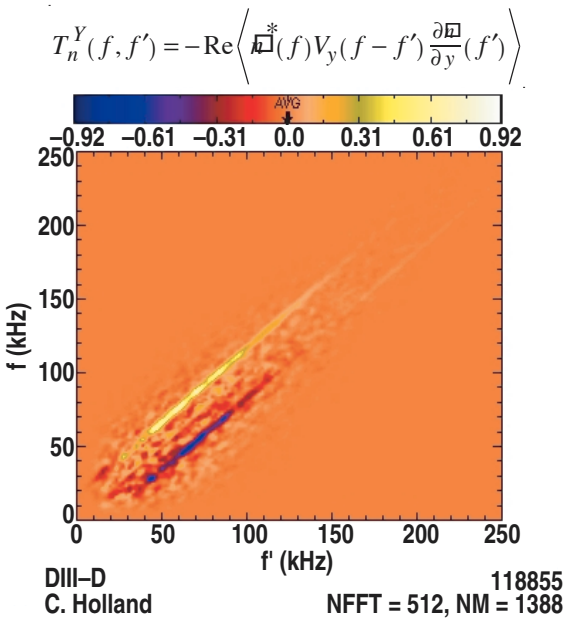

Fig. 9. Plot of $T_n^y(f, f')$ computed from BES data taken on DIII-D. Because of limitations on the measurement of V_y by correlation techniques, only the diagnonal band in the middle of the plot contains significant data. Plot shows forward cascade to higher frequency mediated by the GAM.

These data provide preliminary answers to the two questions posed at the beginning of this section. Considering all the experimental data, there is significant evidence that zonal flows exist in toroidal plasmas. In addition, there is evidence that both the zonal flows and GAMs can affect the higher frequency turbulence. There are, however, still some holes in the experimental results. It would be extremely useful to have an experimental demonstration in tokamak plasmas that the zonal flow candidates really do satisfy the $n = 0$ toroidal uniformity prediction. Likewise missing is the detection of the m/n = 1/0 pressure fluctuation associated with the GAM. (The measurements to date have all been done at the midplane of the plasma where the pressure fluctuation is zero.)

III. SPATIAL SPREADING OF TURBULENCE

Spatial spreading of turbulence refers to a process where turbulence spreads from one region of the plasma where it is generated to a second region where the turbulence drive is smaller or nonexistent [20-23]. Accordingly, the free energy that drives the turbulence in one location can cause turbulent transport in another location. Turbulence spreading can have several important effects. First, along with profile shearing, turbulence spreading can lead to broken gyroBohm scaling [22]. Second, as has been recently discussed [24,25], spreading can produce enhanced transport even in transport barriers where local calculations would indicate that turbulence is suppressed. Third, turbulence spreading could allow edge turbulence to contribute to core transport.

Key experimental questions in this area are:

1. Can we determine unique experimental signatures of turbulence spreading so that we can identify it in the experimental data?
2. Do we have data demonstrating turbulence spreading?

Recent results from JT-60U provide some data that is superficially consistent with turbulence spreading [26]. However, other results from the same discharges make the picture considerably murkier. In these experiments, turbulent density fluctuations were measured via reflectometry in discharges with box-type internal transport barriers (ITBs). Some of the results are shown in figure 10. The most important result for turbulence spreading is the presence of finite amplitude density fluctuations near the magnetic axis [figure 10(a)], in a region where the turbulence stability calculations with the FULL code [27] indicate that electrostatic microturbulence is stable [figure 10(b)]. The flat profiles of density [figure 10(a)] and electron and ion temperature (not shown) in this region inside the ITB also suggest the presence of significant turbulent transport. The presence of broadband density fluctuations in a region where microturbulence is calculated to be stable might be explained by turbulence spreading.

In assessing turbulence spreading, we need to be aware that there is substantial amount of turbulence physics active in the final, saturated turbulent state that is not included in electrostatic linear stability calculations such as those in the FULL code [27]. As is illustrated in figure 11, there can be substantial variations in the inferred plasma transport across the region where the turbulence is calculated to be linearly unstable [28]. The shaded region in figure 11 encompasses the whole linearly unstable region shown in

figure 11. Across this linearly unstable region, the inferred transport drops by roughly a factor of 50 for both the electrons and ions. Since we believe that the higher levels of transport for $R \geqq 3.85$ m are due to turbulence, we see that this turbulence-driven transport can change dramatically even in a region where the turbulence is calculated to be linearly unstable. This variation might be due to something like the Dimits shift, which is related to zonal flow effects near marginal stability [29]. This variation in turbulent transport across the linearly unstable region indicates that we need a better criterion than linear instability for electrostatic modes to determine the spatial regions where turbulence is important. Until we know the regions where turbulence is important, it is difficult to look for the effects of spreading.

The electrostatic linear stability may be too crude a measure for another reason. There are modes in the plasma that can affect the transport which are not included in the usual electrostatic calculations. Shown in figure 12 is a case where the onset of toroidal Alfvén eigenmodes (TAE) is correlated with substantial drops in ion temperature and rotation in a DIII-D L-mode shot with an ITB [30]. Local density fluctuation measurements made in the plasma core using beam emission spectroscopy (BES) show the onset of the harmonic structure characteristic of the TAE. Ion temperature and rotation in regions near and inside the BES measurement location clearly drop when the TAE starts. The TAE ceases when $q_{\min}$ reaches two [30].

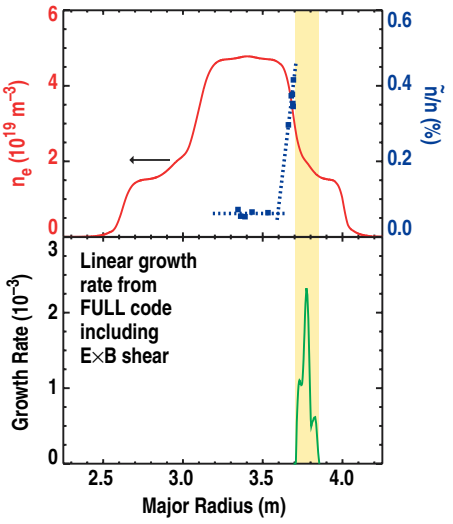

Fig. 10. Inferred density fluctuation level (blue) and the plasma density profile (red) in the internal transport barrier plasma in JT-60U compared to the calculated linear growth rate (bottom) using the FULL code including the effects of rotation (green). The calculated linear growth rate is only plotted in the region where there are reflectometer measurements. The yellow shading shows the region where the FULL code predicts linear instability.

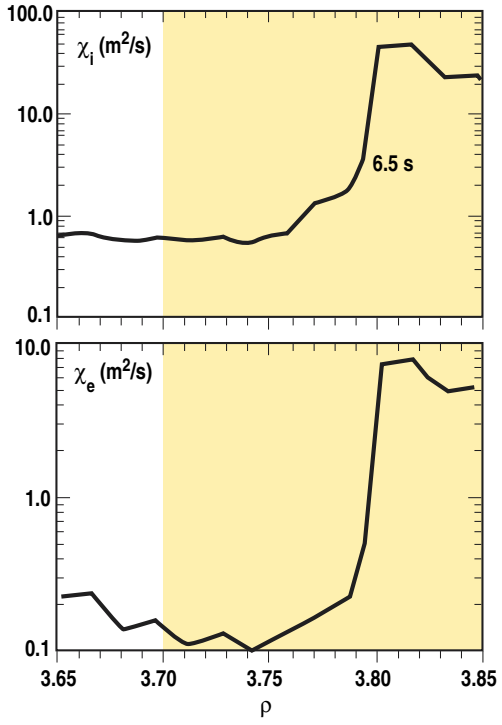

Fig. 11. Ion thermal diffusivity (a) and electron thermal diffusivity (b) plotted as a function of major radius for the JT-60U shot shown in Fig 10. The yellow shading covers the same region as shown in Fig. 10. Note that the diffusivities fall abruptly in the middle of the region of linear instability.

Another way to look for turbulence spreading is to exploit edge transport barrier formation at the L to H transition or edge barrier collapse at the H to L transition to provide a situation where the edge turbulence changes rapidly. One can then look for associated changes in the turbulence at locations further inside the plasma to see whether there is evidence for spreading. Data in figures 13 and 14 from a well-documented L to H transition in DIII-D [31] can be used to look for evidence of spreading. As is shown in figure 13, the edge density fluctuations change abruptly at the time of the L to H transition, just when the divertor D_α emission changes. As is shown in figure 14, this change in density fluctuations takes place in a narrow region near the separatrix; this is the same region where the gradients steepen and the radial electric field well develops in the H-mode edge plasma. As can be seen in figure 14, there is no change in the density fluctuations across the L to H transition inside of $R = 2.28$ m. Accordingly, in this case, we do not see any signature of turbulence spreading. Had turbulence spreading taken place, one would have expected to see a reduction in density fluctuations inside the region where the steep edge gradients and the radial electric field well develop. Of

course, this result simply says that turbulence spreading does not exist in this case; the experimental results do not forbid its occurrence in other cases.

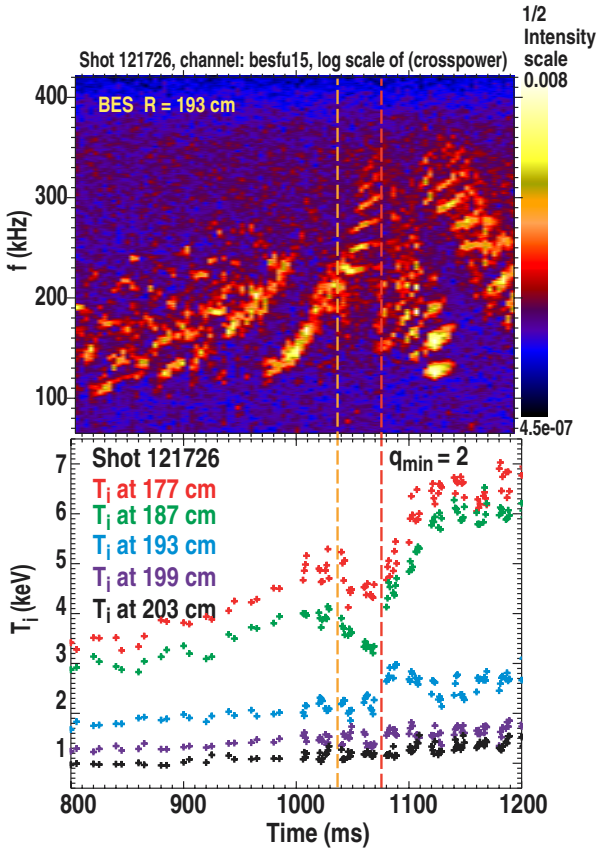

Fig. 12. Upper box shows color coded frequency spectrum as a function of time measured with the DIII-D BES system showing the effect of reverse shear Alfvén modes (prior to the yellow dashed vertical line at 1035 ms) and toroidal Alfvén eigenmodes (between the dashed vertical lines). The second orange vertical line shows the time when the minimum value of q reaches 2. The lower box shows the ion temperature at various radii as a function of time. Note that there is a correlation between the presence of the toroidal Alfvén eigenmodes and the drop in ion temperature. Toroidal rotation also drops at this time.

In order to make further progress in this area, we need to determine unique signatures of turbulence spreading that can be quantified and measured experimentally. This will almost certainly involve comparing radial profiles of turbulence amplitudes with the amplitudes that would be expected based on just the local gradients in the plasma parameters. Establishing this local response amplitude will be a significant challenge for both theory and experiment. Experiments exploiting time dependence (such as in the L to H transition case just discussed) can add an additional dimension to the investigation.

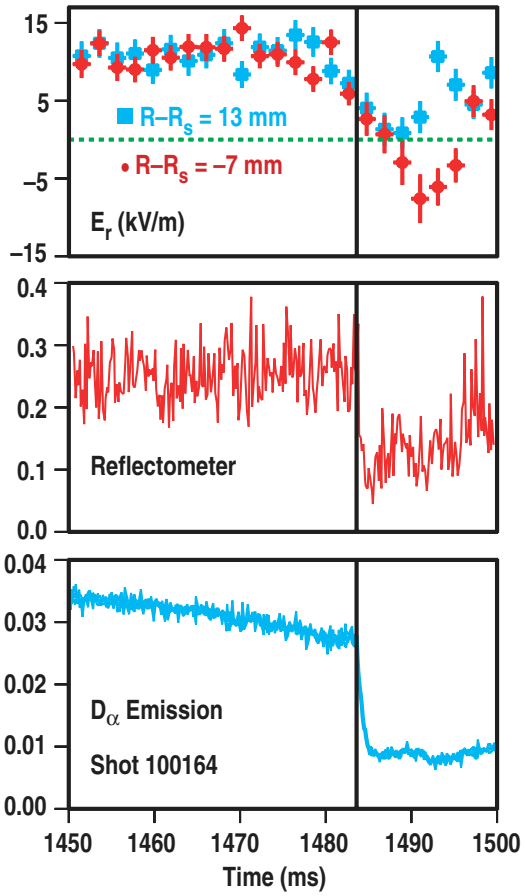

Fig. 13. Time history across an L-H transition in DIII-D showing changes in (a) radial electric field, (b) density fluctuations from reflectometry and (c) divertor D_α emission. Note that E_r begins to change slightly before the time of the transition as indicated by the drop in the reflectometer and D_α signals.

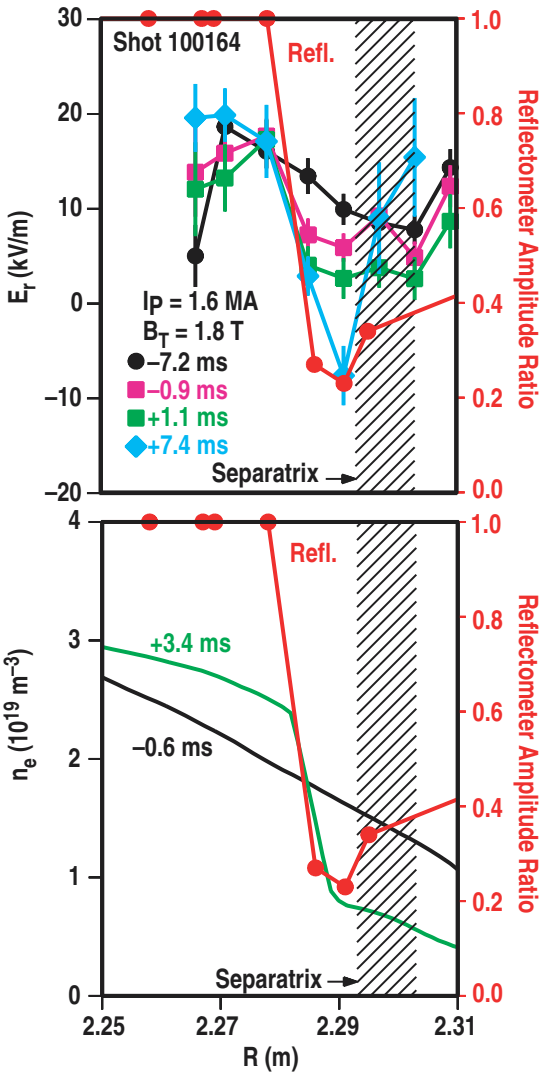

Fig. 14. E_r and density profile across the L to H transition for the same shot as in Fig. 13 showing the formation of the E_r well and the steepening of the edge density gradient characteristic of the H-mode. The ratio of reflectometer density fluctuations before and after the transition is shown in red (right hand scale). This ratio drops by a factor of about five for locations outside R = 2.28 m, indicating significant reduction in turbulent density fluctuations; however, there is no change in this ratio for locations inside R = 2.28 m.

IV. SHORT WAVELENGTH TURBULENCE

In ITBs, it is quite common to find ion thermal diffusivity reduced to the neoclassical level. Indeed, this is sometimes used as a definition of the presence of an ITB. This reduction is consistent with the idea that ion temperature gradient (ITG) turbulence has been suppressed owing to $E \times B$ shear [1]. In some ITBs, electron thermal transport and particle transport are also reduced. However, in many other cases, these latter transport channels are essentially unchanged. Electron thermal transport is the transport channel that is most difficult to affect. This different behavior of the ion and electron thermal transport strongly suggests that electron thermal transport can be driven by modes other than ITG.

Theory indicates that shorter wavelength turbulence modes such as trapped electron mode (TEM) and electron temperature gradient modes (ETG) can drive electron thermal transport. However, there are conflicting predictions whether ETG can drive significant transport [32,33] or not [34-37]. The different behavior of electron thermal and ion thermal transport in ITBs and the theoretical disagreement over the magnitude of ETG-induced transport both motivate experimentalists to measure shorter wavelength turbulence.

The approximate spatial scales of ITG are in the range $0.1 \lesssim k_\perp \rho_i \lesssim 0.5$ while TEM is in the range $0.5 \lesssim k_\perp \rho_i \lesssim 1$ and ETG is in the range $0.8 \lesssim k_\perp \rho_i \lesssim 10$. Accordingly, ETG measurements require measuring turbulence on spatial scales around a factor of 10 smaller than ITG measurements.

Recent advances in microwave scattering [38-41] and far infrared scattering [38,39] allow measurements in the ETG range of $k_\perp \rho_i$, although the scattering geometry tends to weight the measurements more to radial than poloidal wavenumbers.

Recent measurements have demonstrated the existence of density turbulence at the small scales characteristic of ETG modes. As is illustrated in figure 15, both a low frequency, low wavenumber mode and a high frequency, high wavenumber mode are seen in the FT-2 tokamak [40,41] at different radial locations. As can be seen in figure 16, measurements in the DIII-D tokamak also demonstrate the existence of high k turbulence in the plasmas which responds to short pulses of neutral beam injection. In both plasmas, ITG and ETG modes are both predicted to be unstable. The fact that turbulence at the ETG scale has been seen in two tokamaks under quite different

conditions utilizing quite different microwave scattering techniques lends extra credence to the observations. However, although ETG modes are predicted to be unstable in these plasmas and to exist at the spatial scales measured, considerable work still remains to demonstrate that the fluctuations seen actually are ETG modes.

A more fundamental issue with short wavelength turbulence measurements is that we will probably have only density fluctuation measurements for the forseeable future. These are insufficient to directly determine the level of transport driven by turbulence of a given spatial scale. Accordingly, to make further progress in this area, we need to develop ways to combine the gyrokinetic code results and the experimental measurements so that we can separate the transport effects of ITG, TEM and ETG modes.

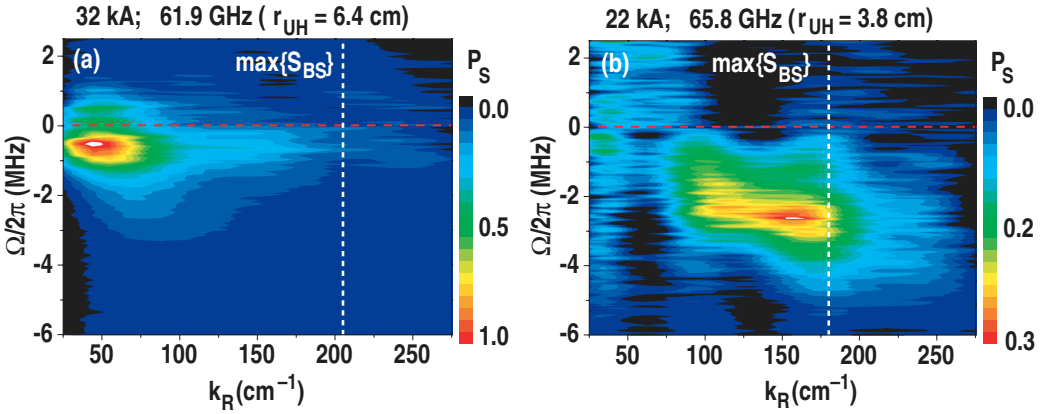

Fig. 15. Color-coded contour plots of density fluctuations measured in the FT-2 device as a function of frequency and wavenumber. For the plasmas cited, $k_R = 200\ \mathrm{cm}^{-1}$ corresponds to $k_R \rho_i \simeq 15$.

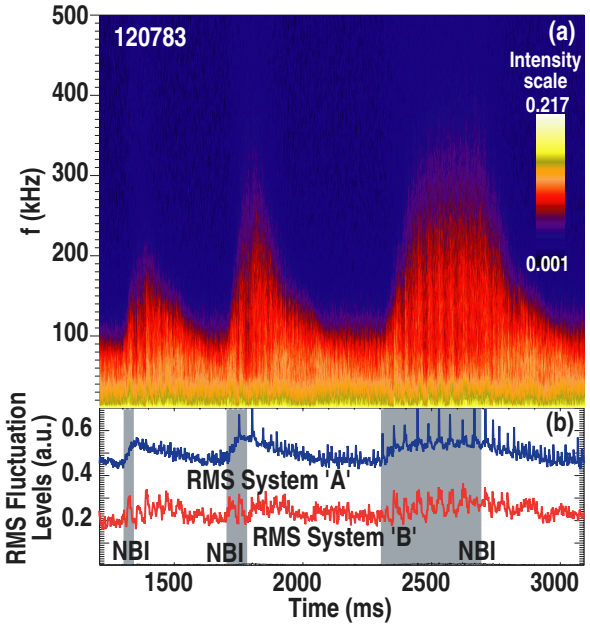

Fig. 16. Color-coded contour plot of frequency spectrum of high k density fluctuations in DIII-D plotted as a function of time in the upper box. The lower box shows frequency integrated fluctuation amplitudes measured by two different microwave backscattering systems. The grey bars in the lower box show the periods when neutral beams are injected. Notice there are significant changes in high k fluctuations each time the neutral beams are on. These measurements are for k = 35 cm^{-1}, which is approximately $k\rho_i$ = 10.

REFERENCES

[1] P W Terry 2000, Rev. Mod. Phys. **72**, 109

[2] P H Diamond, S-I Itoh, K Itoh, and T S Hahm 2005, Plasma Phys. Control. Fusion **47**, R35

[3] A Fujisawa, K Itoh, H Iguchi, K Matsuoka, S Okamura, A Shimizu, T Minami, Y Yoshimura, K Nagaoka, C Takahashi, M Kojima, H Nakano, S Ohsima, S Nishimura, M Isobe, C Suzuki, T Akiyama, K Ida, K Toi, S-I Itoh, and P H Diamond 2004, Phys. Rev. Lett. **93**, 165002-1

[4] A Fujisawa, A Shimizu, H Nakano, S Ohsima, K Itoh, H Iguchi, K Matsuoka, S Okamura, S.-I. Itoh, and P.H. Diamond, "Properties of Turbulence and Stationary Zonal Flow on Transport Barrier in CHS," submitted to Plasma Phys. and Control. Fusion (2005) this conference.

[5] A Fujisawa, A Shimizu, H Nakano, S Ohsima, K Itoh, H Iguchi, Y Yoshimura, T Minami, K Nagaoka, C Takahashi, M Kojima, S Nishimura, M Isobe, C Suzuki, T Akiyama, Y Nagashima, K Ida, K Toi, T Ido, S-I Itoh, K Matsuoka, and S Okamura, P H Diamond, "Turbulence and Transport Characteristics of a Barrier in a Toroidal Plasma," submitted to Plasma Phys. Control. Fusion (2005)

[6] Y Nagashima, K Hoshino, A Ejiri, K Shinohara, Y Takase, K Tsuzuki, K Uehara, H Kawashima, H Ogawa, T Ido, Y Kusama, and Y Miura 2005, Phys. Rev. Lett. **95**, 095002

[7] H Y W Tsui, P M Schoch, and A J Wootton 1993, Phys. Fluids B **5**, 1274

[8] Y Hamada, A Nishizawa, Y Kawasumi, A Fujisawa, H Iguchi and JIPP T-IIU Group 1997, Fusion Eng. and Design **34-35**, 657 (1997)

[9] Y Hamada, A Nishizawa, Y Kawasumi, A Fujisawa, H Iguchi 1997, Fusion Eng. and Design **34-35**, 663 (1997)

[10] P M Schoch, K A Connor, D R Demers and X Zhang 2003, Rev. Sci. Instrum. **74**, 1846

[11] A V Melnikov, L G Eliseev, A V Gudozhinik, S E Lysenko, A V Mavrin, S V Perfilov, L G Zimeleva, M V Ufimtsev, L I Krupink and P M Schoch 2005, Czech. J. Phys **55**, 349

[12] G D Conway, B Scott, J Schirmer, M Reich, A Kendl and the ASDEX Upgrade Team 2005, Plasma Phys. Control. Fusion **47**, 1165

[13] G R McKee et al. 2004, Rev. Sci. Instrum. **75**, 3490

[14] M Jakubowski, R J Fonck and G R McKee 2002, Phys. Rev. Lett. **89**, 265003

[15] G R McKee, R J Fonck, M Jakubowski, K H Burrell, K Hallatschek, R A Moyer, D L Rudakov, W Nevins, G D Porter, P Schoch, and X Xu 2003, Phys. Plasmas **10**, 1712

[16] G R McKee, R J Fonck, M Jakubowski, K H Burrell, K Hallatschek, R A Moyer, D L Rudakov, and X Xu 2003, Plasma Phys. and Control. Fusion **45**, A477

[17] G R McKee, D K Gupta, R J Fonck, D J Schlossberg, M W Shafer, P Gohil 2005, "Structure and Scaling Properties of the Geodesic Acoustic Mode," submitted to Plasma Phys. and Control. Fusion

[18] D K Gupta, G R McKee need the complete reference

[19] C Holland, G R Tynan, R J Fonck, G R McKee, R E Waltz, J Candy 2005, "Quantitative Studies of Nonlinear Interactions Between Shear Flows and Turbulence in Experiment and Simulation," Bull. Am. Phys. Soc. **50**, QP1.00030

[20] T S Hahm, P H Diamond, Z Lin, K Itoh and S-I Itoh 2004, Plasma Phys. and Control. Fusion **46**, A323

[21] O Gurcan, P H Diamond, T S Hahm, Z Lin 2005, Phys. Plasmas **12**, 032303

[22] R E Waltz and J Candy 2005, Phys. Plasmas **12**, 072303

[23] T S Hahm, P H Diamond, Z Lin, G Rewoldt, O Gurcan and S Ethier 2005, Phys. Plasmas **12**, 090903

[24] T S Hahm, P H Diamond, W Wang, G Rewoldt, O Gurcan and Z Lin 2005, "Effect of Shear Flows on Turbulence Spreading," submitted to Plasma Phys. and Control. Fusion (this conference)

[25] M Yagi, T Ueda, S-I Itoh, M Azumi, K Itoh, T S Hahm and P H Diamond 2005, "Turbulence Spreading in the Presence of ITB," submitted to Plasma Phys. and Control. Fusion (this conference)

[26] R Nazikian, K Shinohara, G J Kramer, E Valeo, K Hill, T S Hahm, G Rewoldt, S Ide, Y Koide, Y Oyama, H Shirai, and W Tang 2005, Phys. Rev. Lett. **94**, 135002-1

[27] G Rewoldt, K W Hill, R Nazikian, W M Tang, H Shirai, Y Sakamoto, Y Kishimoto, S Ide, T Fujita 2002, Plasma Phys. Control. Fusion **42**, 403

[28] R Nazikian, R Budny 2005, Princetion Plasma Physics Laboratory, private communication

[29] A M Dimits, G Bateman, M A Beer, B I Cohen, W Dorland, G W Hammet, C Kim, J E Kinsey, M Kotchenreuther, A H Kritz, L L Lao, J Mandrekas, W M Nevins, S E Parker, A J Redd, D E Shumacher, R Sidora and J Weiland 2000, Phys. Plasmas **7**, 969

[30] M E Austin et al. "Core Barrier Formation Near Integer q Surfaces in DIII-D," submitted to Phys. Plasmas (2005).

[31] K H Burrell 2001, Rev. Sci. Instrum. **72**, 906

[32] F Jenko, W Dorland, M Kotschenreuther, B N Rogers 2000, Phys. Plasmas **7**, 1904

[33] F Jenko, W Dorland 2002, Phys. Rev. Lett. **89**, 225001-1

[34] B Labit, M Ottaviani 2003, Phys. Plasmas **10**, 126

[35] J Li, Y Kishimoto 2004, Phys. Plasmas **11**, 1493

[36] Z Lin, L Chen, and F Zonca 2005, Phys. Plasmas **12**, 056125-1

[37] O D Gurcan and P H Diamond 2004, Phys. Plasmas **11**, 4973

[38] T L Rhodes, W A Peebles, M vanZeeland, D Mikkelsen, M A Gilmore, X V Nguyen, D R Baker, J C DeBoo, J S deGrassie, W Dorland, E J Doyle, C M Greenfield, C C Petty, and L Zeng, "Comparison of Broad Spectrum Turbulence Measurements and Gyrokinetic Code Predictions on the DIII-D Tokamak," IAEA CN/EX/P6-23, http://www-pub.iaea.org/MTCD/Meetings/PDFplus/fusion-20-preprints/EX_P6-23.pdf

[39] T L Rhodes, W A Peebles, M A VanZeeland, J S deGrassie, G R McKee, G M Staebler, J C DeBoo, E J Doyle, M Gilmore, P Gohil, C M Greenfield, R J Groebner, X V Nguyen, G Wang, and L Zeng 2005, "First Measurements of Density Turbulence Below the Ion Gyroscale on DIII-D," submitted to Phys. Rev. Lett.

[40] E Z Gusakov, A D Gurchenko, A B Altukhov, A Yu Stepanov, L A Espinov, M Yu Kantor, D V Kouprienko, "First Observation of ETG Mode Component of Tokamak Plasma Turbulence by Correlative UHR Backscattering Diagnostics," Proc. of 32nd EPS Conf. on Plasma Physics and Controlled Fusion, Tarragona, Spain 2005, (European Physical Society, 2005) http://eps2005.ciemat.es

[41] A D Gurchenko, E Z Gusakov, A B Altukhov, A Yu Stepanov, L A Esipov, M Yu Kantor, D V Kouprienko 2005, "Investigation of ETG Mode-Scale Component of Tokamak Plasma Turbulence by Correlative Enhanced Scattering Diagnostics," submitted to Plasma Phys. and Control. Fusion (this conference).

ACKNOWLEDGMENT

This work was supported in part by the U.S. Department of Energy under DE-FC02-04ER54698. This paper is based on a presentation given at the Tenth IAEA Technical Committee Meeting on H-mode Physics and Transport Barriers and benefited from presentations and discussions held at that meeting. I would especially like to thank P.H. Diamond for his comments on zonal flows and turbulence spreading. In addition, I thank all the individuals who provided the figures used in this work.